Lasing-Encoded Microsensor Driven by Interfacial Cavity Resonance Energy Transfer

Zhiyi Yuan [1], *Ziyihui Wang* [2], *Peng Guan* [2], *Xiaoqin Wu* [3], and *Yu-Cheng Chen* [1,4] *

[1] Zhiyi Yuan, Prof. Yu-Cheng Chen

School of Electrical and Electronics Engineering, Nanyang Technological University, 639798, Singapore

[2] Ziyihui Wang, Peng Guan

School of Precision Instrument and Opto-Electronics, Tianjin University, Tianjin, 22, China

[3] Dr. Xiaoqin Wu

Department of Biomedical Engineering, University of Michigan, Ann Arbor, 48109, USA

[4] Prof. Yu-Cheng Chen

School of Chemical and Biomedical Engineering, Nanyang Technological University, 639798, Singapore

*Correspondence E-mail: yucchen@ntu.edu.sg

Keywords: laser, whispering-gallery mode, molecular sensing, interface, energy transfer

Abstract—

Microlasers are emerging tools for biomedical applications. In particular, whispering-gallery-mode (WGM) microlasers are promising candidates for sensing at the bio-interface owing to their high quality-factor and potential in molecular assays, and intracellular and extracellular detection. However, lasing particles with sensing functionality remains challenging since the overlap between the WGM optical mode and external gain medium is much lower compared to internal gain inside the cavity. To overcome this problem, the concept of Förster resonant energy transfer (FRET) was exploited on WGM droplet microlaser by separating donor and acceptor molecules at the cavity-surface interface. It was first discovered that the interfacial FRET laser not only originated from conventional FRET but utilizes coherent radiative energy transfer (CRET) to excite acceptor molecules by inducing light-harvesting effect near the cavity interface. Simulations and experiments have revealed that the absorption spectrum of individual analyte plays a crucial role in interfacial FRET laser. Distinct lasing spectra could therefore distinguish molecules of different absorption properties upon binding. Finally, detection of small fluorescent molecules and photosynthetic protein was performed. The results presented here not only demonstrate the wide-ranging potential of microlaser external cavity implementation in molecular sensing applications, but also provide comprehensive insights into cavity energy transfer in laser physics.

1. Introduction

Microlasers have emerged as a promising technology, garnering a tremendous amount of attention owing to its potential for use in biomedical and biological applications [1-5]. Various types of optical micro-cavities have been developed, such as Fabry-Perot cavities[6-8], photonic crystals[9], and whispering-gallery-modes (WGMs), as implemented in ring resonators[10-12], micro/nano disks [13-14], and microspheres [3-5, 15-20]. In particular, microsphere-based WGM lasers are appealing candidates for sensing probes owing to their convenience, extremely high Q factor, and potential for application in intracellular and extracellular probes [13, 15-16, 21-22]. Moreover, analytes can be positioned outside of the optical cavity, where an evanescent field exists at the external interface between the resonant cavity and surrounding medium [23-25]. At present, most microsphere or droplet-based WGM lasers are considered to be passive-detection devices, as they require physical changes (e.g., refractive indexes) to induce a resonance spectral shift, and thus cannot provide detailed biochemical information [26-28]. In contrast, active-detection devices, which employ analytes as the gain medium, can provide more selective and sensitive information about the bio-species [8, 29]. Therefore, the ability to utilize a biological gain medium on the external surface of a microsphere cavity will allow us to amplify subtle changes in the gain medium and the resultant spectra, threshold, and lasing modes. However, the overlap factor for the optical mode and gain medium is much lower than the value of the gain within the cavity, and the background fluorescence also interferes with the external cavity sensing, making this amplification a difficult task. Thus, to enable amplification of these subtle changes, we have applied the concept of Förster resonance energy transfer (FRET) at the interface of a droplet-based laser to separate the donor and acceptor at the droplet-surface interface (**Figure 1a**). FRET is an electrodynamic phenomenon that is highly sensitive to distance, spectral overlap, and

the orientation between donor and acceptor molecules. In the past decade, FRET has been used as a powerful tool for providing nanoscale information in many biosensing applications. The performance of FRET is mainly dependent on the design of the donor and acceptor pairs. Several groups recently utilized FRET by using donor molecules as exciton funnels [30-31], or light-harvesting antennas [31], to realize a wavelength tunable laser [30], single molecule nanoprobes [32], or light redirectioning devices [33] that strongly amplify the emission of acceptor molecules when the number of donor molecules far exceed the total number of acceptor molecules. As such, implementation of FRET in a microlaser can not only yield a much stronger signal-to background ratio and higher sensitivity than the conventional FRET fluorescence-based method, but, more importantly, can also enhance the functionality of the microlaser sensor. As with evanescent field coupling, the FRET effect can occur at the interface under the condition of relatively short distance between the acceptor molecules and resonant cavity surface. Besides the FRET effect, acceptor molecules can be excited to higher energy level by the photons emitted by the donor inside the droplet to form lasing, where we define it as coherent radiative energy transfer (CRET), as shown in Figure 1b.

Inspired by such unique phenomena, we propose an interfacial FRET laser that utilizes the liquid crystal (LC) microdroplet cavity. In addition to the FRET effect, the combination of an extremely high concentration of donor dye inside the cavity and light-harvesting antenna phenomena enables CRET-induced excitation (Figure 1c). By exploiting both effects, external cavity laser sensing was achieved, and the lowest molecular (acceptor) concentration at which lasing was achieved was 25 μM. We also found that, by gradually increasing the acceptor molecule concentrations, the laser signal from the donor could be significantly affected, and eventually eliminated. We further discovered that molecule-coated microdroplets could achieve lasing with a

significantly lower (i.e., three times lower) lasing threshold, indicating that the molecules on the surface layer and surrounding medium can both contribute to the realization of an interfacial FRET laser. The characteristics of such an interfacial FRET laser were investigated by performing simulations and experiments with various acceptor/donor concentrations, cavity sizes, and molecules. Our results demonstrate that the absorption of an individual analyte (acceptor) plays a critical role in interfacial FRET laser, confirming that different molecules can be encoded according to distinct lasing spectra; thus, devising the concept of a lasing-encoded microsensor. We also demonstrate protein detection with an R-phycoerythrin (RPE) interfacial FRET laser. These results not only open a door to broad range of biomedical sensing applications, but also provide comprehensive insight into interfacial energy transfer in laser physics.

2. Results and Discussion

2.1. Demonstration of interfacial FRET laser

To begin, we first explored the possibility of achieving FRET laser/fluorescence emission by separating the donor molecules and acceptor molecules at the interface of a liquid crystal microcavity (Diameter, 25 μm; Donor concentration, 20 mM for all the experiments in this work). Two configurations were investigated, as shown in Figure 1a; in these configurations, the donor and acceptor can be placed inside or outside of a microcavity. **Figure 2a**, corresponding to Configuration 1, depicts the dynamic lasing spectra of a fixed Coumarin 6 (C6, donor) microdroplet that were obtained by gradually dropping 0.1-mM Rhodamine B (RhB, acceptor) molecules onto the external surface. The intensity of the donor (C6) lasing peaks significantly decreased over time, whereas the

new lasing peaks associated with FRET emerged near 590 nm. It can be seen that increasing the acceptor (RhB) concentration to 0.5 mM resulted in the strong absorption of RhB eliminating the C6 donor lasing peaks. As the RhB concentration increased, the donor lasing peaks decayed at a faster rate, as shown in Figure 2b. In the proposed system, because a high concentration of C6 molecules are encapsulated in the microdroplet, there is a higher probability that C6 molecules will be present in the coherence and stimulated emissions. In contrast, most RhB molecules are not present in the stimulated emission because the evanescent wave penetration depth is considered to be much smaller than the height of the RhB solution surrounding the microdroplet. SI Figure 1 shows the RhB fluorescence to be stronger than the C6 fluorescence; this is because large amounts of spontaneous photons were emitted from the high concentration of RhB molecules surrounding the microdroplet. Figure 2d shows the FRET lasing emission spectra for various pump energy densities; a threshold of 12 μJ/mm^2 was observed (Figure 2e). In contrast, lasing was found to be impossible without donor C6 (SI Figure 2). Interestingly, the number of modes was found to be independent of the pump energy density; this observation is uncharacteristic of multi-modal WGMs. In fact, our interfacial FRET laser operates outside of the microdroplet, where only a few modes can contribute to interfacial FRET lasing.

We further investigated whether the light-harvesting effect exists when the acceptor is positioned within the resonant cavity (i.e., Configuration 2). Figure 2c shows the dynamic lasing spectra of a fixed Nile Red (NR, acceptor) microdroplet that were obtained by gradually adding 0.5-mM Fluorescein isothiocyanate (FITC, donor) solution. Unlike the conditions that yielded the results shown in Figure 2a, the acceptor (NR) dye molecules were enclosed within the cavity, and the donor (FITC) molecules were located on the external cavity surface. Additionally, there was no significant

change in the NR lasing peaks because of the following two reasons. First, even though the cross section of NR molecule absorption was higher at the FITC emission wavelength than at the pump excitation wavelength, the pump photons were absorbed by FITC molecules and re-emitted via directionless spontaneous emission, ensuring that the total pump energy received by NR did not increase. Second, the number of donor molecules was lower than that of acceptor molecules; hence, the amount of pump energy from FRET was much lower than that from the optical pump. Figure 2f shows the spectrally integrated NR laser output as a function of pump energy density (640–660 nm). The results prove that the donor outside of the cavity minimally affects the lasing behavior of the acceptor, which is consistent with what can be observed in the results shown in Figure 2c.

To confirm that the lasing peaks ranging from 580 to 610 nm are related to interfacial FRET, we prepared an LC microdroplet without any doped dye, and recorded the spectra after adding 0.5 mM of RhB solution. The only occurrences of fluorescence emission associated with RhB were detected at excitation wavelengths of 450 nm and 532 nm (SI Figure 2a–b). Interestingly, because of cavity-enhanced spontaneous emission, we only observed a modulated fluorescence signal under the condition of extremely high pump energy density and an excitation wavelength of 532 nm. Generally, to achieve lasing when gain molecules are positioned outside of the WGM cavity, a higher threshold and gain concentration are required to offset the extremely small overlap between the optical mode and external surface gain medium. These drawbacks strongly discourage the application of external cavity microlasers as biosensors. As such, we discovered that the CRET (Figure 1b) and FRET effects are indispensable in interfacial FRET laser technology, which entails a high-concentration of donor molecules inside the microdroplet acting as a light-harvesting antenna.

2.2. Lasing with cavity-interface coated molecules

Next, we comprehensively investigated the role of the interfacial cavity effect in FRET laser emission. Because WGM only occurs at the cavity interface, we coated a monolayer of RhB (acceptor) molecules on the surface of C6 (donor) microdroplets and conducted lasing experiments that are similar to that described above. Detailed methods for coating can be found in Methods section. The red-colored sphere periphery that can be observed in **Figure 3a** denotes red fluorescence emission from RhB molecules on the cavity surface, and it is shown for coated and non-coated microdroplets; note that green fluorescence from the C6 microcavity is not presented here. The red background is the product of the remaining RhB molecules in the surrounding solution. Figure 3b presents a comparison of the lasing threshold for microdroplets with and without coated RhB molecules, and with extremely low RhB acceptor concentrations. It was discovered that the lasing threshold for RhB-coated microdroplets was three times lower than that for non-coated microdroplets, and under the condition of a concentration as low as 15 μM. Therefore, it is very clear that the characteristics of the interfacial FRET laser are largely determined by the surface-adsorbed RhB molecules. At a very low RhB concentration, RhB-coated microdroplet was found to have a much lower threshold than the microdroplet without coating; this is because the single layer of RhB molecules was designed to have an effective volume concentration within the range of 5 to 10 μM. Additionally, the downward trend of the coated microdroplet threshold was slower than that of the normal microdroplet, demonstrating that the surface of the coated microdroplet reached saturation, causing the increasing RhB solution concentration to only minimally increase the surface density of the RhB molecules. Furthermore, when the surrounding RhB solution concentration was high, the RhB-coated microdroplet was found to have a higher threshold than that of the normal

microdroplet because of the longer distance (D-A pair) generated by the PSS (Poly4-styrenesulfonic acid) molecules on the microdroplet surface. To illustrate the effects of coating on lasing performance, we compared the lasing spectra for coated and non-coated microcavities under the condition of low or high concentration (Figure 3c and d). At a very low concentration (15 μM RhB), no lasing spectra were observed for the microdroplet without a surface coating; this observation is consistent with the results shown in Figure 3b. In contrast, owing to the gain of the coated surface, sharp lasing emission was observed for the coated microdroplet. However, at higher concentrations (100 μM RhB), no obvious difference was observed, as can be seen in Figure 3d.

2.3. Theoretical and experimental analyses of interfacial laser results

The above-described results indicate an important feature of this interfacial FRET laser, which is the amount of monolayer acceptor molecules adsorbed on the microdroplet interface is very significant. Because the distance between acceptor molecules and donor molecules is extremely short (i.e., typically shorter than the 0.5 Förster distance), such molecules are expected to have a remarkably high resonance energy transfer rate. However, our results, as illustrated in Figure 3 (RhB-coated microdroplets), confirm that the energy transferred from FRET itself is not sufficient to achieve population inversion. This finding supports the possibility of CRET contribution, which may be the dominant source of energy for an interfacial FRET laser. Given that most acceptor molecules in the surrounding solution only produce background fluorescence (instead of coherence- and stimulated-emission photons), we discovered that they play an important role in interfacial FRET laser function. To further investigate these characteristics, we simulated the interfacial FRET lasing

threshold by employing a rate equation composed of coupled differential equations to describe the population dynamics of excited state molecules density and photons density of donor and acceptor, as described by Equations (1) to (4). The first terms on the right-hand side of Equations (2) and (4) were derived based on the spontaneous emission of the excited dye molecules [34]. The first three terms on the right-hand side of Equation (3) were derived based on the direct excitation of optical pump, the FRET from donor to acceptor, and the CRET from donor to acceptor. According to the first and third terms, the surrounding acceptor dye solution significantly contributes to the interfacial FRET lasing behavior.

$$\frac{dn_d(t)}{dt} = I_p(t)|abs_d|\big(N_d - n_d(t)\big) - k_F n_d(t) - \frac{cq_d(t)}{m_1}\Big(\sigma_{de} n_d(t) - \sigma_{da}\big(N_d - n_d(t)\big)\Big) - \frac{n_d(t)}{\tau_d} \quad (1)$$

$$\frac{dq_d(t)}{dt} = \frac{cq_d(t)}{m_1 V} n_d(t) + \frac{cq_d(t)}{m_1}\Big(\sigma_{de} n_d(t) - \sigma_{da}\big(N_d - n_d(t)\big)\Big) - \frac{cq_d(t)}{m_1}\delta_{aa}\big(N_a - n_a(t)\big) - \frac{q_d(t)}{\tau_{cd}}; \quad (2)$$

$$\frac{dn_a(t)}{dt} = I_p(t)|abs_a|\big(N_a - n_a(t)\big) + k_F n_d(t)\frac{+cq_d(t)}{m_1}\delta_{aa}\big(N_a - n_a(t)\big) - \frac{cq_a(t)}{m_2}\Big(\sigma_{ae} n_a(t) - \sigma_{aa}\big(N_a - n_a(t)\big)\Big) - \frac{n_a(t)}{\tau_a}; \quad (3)$$

$$\frac{dq_a(t)}{dt} = \frac{cq_a(t)}{m_2 V} n_a(t) + \frac{cq_a(t)}{m_2}\Big(\sigma_{ae} n_a(t) - \sigma_{aa}\big(N_a - n_a(t)\big)\Big) - \frac{q_a(t)}{\tau_{ca}}; \quad (4)$$

Assuming that only the donor or acceptor can achieve lasing under the condition of a single optical mode, in the above equations, $n_d(t)$, $n_a(t)$, $q_d(t)$, and $q_a(t)$ respectively represent the densities of the donor and acceptor dye molecules in the first excited state, and the densities of the photons emitted by the donor and acceptor dye molecules. $|abs_d|, |abs_a|$ respectively describe the absorption cross sections of the donor and acceptor at the excitation wavelength. σ_{de}, σ_{da}, and δ_{aa} are the donor emission, donor absorption, and acceptor absorption cross sections, respectively, at the donor dye lasing wavelength. σ_{ae} and σ_{aa} are the acceptor emission and acceptor absorption cross sections, respectively, at the acceptor dye lasing wavelength. $I_p(t)$ is the time-dependent pump intensity, and N_d and N_a are the respective concentrations of donor and acceptor dye molecules. m_1 and m_2 respectively represent the resonant cavity and surrounding medium refractive index. k_F is the FRET rate, and τ_d, τ_a, τ_{cd}, and τ_{ca} respectively denote the fluorescence lifetimes of the donor and acceptor, and the cavity decay times of the donor laser and acceptor laser. V is the mode volume.

To validate our theoretical model and conditions for laser-based sensing, we investigated the acceptor and donor concentrations; the results are shown in **Figure 4a** and b, respectively. Figure 4a shows the experimental and simulated results for the interfacial FRET lasing threshold that were obtained by varying the acceptor (RhB) concentrations. Under the condition of very low acceptor molecule concentration, the interfacial FRET lasing threshold rapidly decreased as the surface-analyte concentration increased, indicating that the lasing-encoded microsensor is very sensitive to the binding analyte concentration. Unexpectedly, the above-described theoretical model was found to agree well with the experimental observations. Particularly, in the simulated and experimental results, the lasing threshold was observed to slowly rise under the condition of relatively higher

concentration. The reason for this phenomenon is that the cross section of absorption at the emission wavelength, which reduced the effective absorption quality factor, induced a re-absorption effect. It should be noted that, for interfacial FRET laser, the most critical part of an optical pump is the efficiency of FRET from the donor. Unlike a direct optical pump, a FRET pump, is strongly dependent on the excited donor molecules and FRET rather than the ground-state acceptor molecules. Thus, the probability of population inversion of the acceptor molecules may decrease as the acceptor concentration increases.

Subsequently, we further investigated the interfacial FRET lasing threshold by varying the donor concentration in the cavity under the condition of a fixed acceptor concentration (i.e., RhB = 0.25 mM). The simulated and experimental results for the FRET lasing threshold are illustrated in Figure 4a and b, respectively. Figure 4b shows the simulated results for the FRET lasing threshold as a function of donor concentration. As the donor concentration increased, the contributions of the FRET pump and CRET pump became more significant, thus lowering the lasing threshold. Lasing spectra with different donor (C6) concentrations is displayed in Figure 4c under the same pump energy density of 150 μJ/mm^2. All microdroplets could achieve interfacial FRET laser with the exception of the 1 mM C6 microdroplet. This observation also validates our model. These results indicate that the CRET excitation energy is a critical factor for interfacial FRET lasing of molecules because the FRET distance between donor and acceptor molecules was fixed. Eventually, we explored the minimum cavity size that would allow interfacial FRET lasing; the results are shown in Figure 4d. The corresponding free spectral range (FSR) was also calculated. Considering that the Q-factor was designed to be exponentially dependent on the microdroplet size, the minimum diameter for the lasing-encoded microsensor was determined to be 7 μm.

2.4. Lasing-encoded sensing

Finally, we aim to demonstrate how the interfacial FRET microlaser can be used to encode different molecules. **Figure 5a** illustrates the basic principle of the lasing-encoded microsensor, where different fluorescent molecules exhibit distinctive FRET lasing spectra according to absorption spectrum. As a proof-of-concept, we prepared four fluorophore molecules with different absorption spectra ranging between 530 and 580 nm. As shown in Figure 5b, the normalized absorption spectra of Rhodamine 6G (orange), Rhodamine B isothiocyanate (magenta), Rhodamine B (red), and Texas Red (black) exhibited different spectral overlaps with the donor emission spectrum (C6, green). Because the laser is very sensitive to the absorption coefficient, different acceptor molecules (i.e., A1, A2, A3, A4) were expected to yield distinct FRET lasing spectra. Thus, under the condition of the same pump energy density, we compared the lasing spectra of four different dyes for different acceptor molecules (i.e., A1, A2, A3, A4) as shown in Fig. 5c. Consequently, the donor-acceptor pair spectra overlap integral $\int_0^\infty F_d(\lambda)\varepsilon_a(\lambda)\lambda^4 d\lambda$ was found to be a critical factor that determines the Förster distance. According to the measurements shown in Figure 5b, the spectra overlap between C6 and R6G (A1) is much larger than that between C6 and the other three molecules. Therefore, the lasing peaks related to the donor immediately disappeared, whereas the FRET lasing peaks derived from R6G were emitted in the range of 580 to 600 nm due to the extremely high energy-transfer efficiency. In contrast, interfacial FRET lasing was not achieved when Texas Red served as the acceptor molecule; this is because of the low absorption overlap with donor (C6) emissions.

For further validation, we decided to demonstrate the potential of this interfacial FRET laser by applying lasing-encoded microdroplets for detection of molecules ranging in size from small to large. In addition to small fluorescent molecules (such as RBITC), next we implemented R-

phycoerythrin (RPE), a photosynthetic fluorescent protein derived from red algae, as the target molecules to further demonstrate its potential for application in protein sensing. Figure 5d presents a schematic of the lasing microsensors attached by R-phycoerythrin molecules. In Figure 5e, we present the distinct lasing-encoded spectra of the RPE interfacial FRET laser and C6 microdroplet laser, demonstrating the extraordinary potential for the implementation of such configurations in future biological sensing technology.

3. Conclusion

In this study, we explored a novel concept that was applied to realize the development of active lasing-encoded sensors by taking advantage of the light-harvesting effect at the cavity interface. Furthermore, for the first time, we explored the possibility of realizing FRET lasing performance by separating donor and acceptor molecules at an interface. The results of our investigations reveal the fundamental mechanism of interfacial FRET laser function, which is that the evanescent wave-coupled lasing originates from FRET and CRET within the microdroplet (donor). Theoretical simulations and experiments were conducted to investigate the lasing behavior of microcavities coated with surface gain molecules, and those without a coating, demonstrating the significance of a lasing cavity interface in sensing technology. The detection limit was approximately 20 μM, and the lasing threshold was determined to be on the order of 10 μJ/mm^2. Additionally, the donor-acceptor pair was found to significantly affect interfacial FRET laser operability because of the spectral integral factor. We also demonstrated how such an interfacial FRET laser can be used as a new type of molecular-encoded sensor by employing the proposed technology to detect RhBITC and

RPE molecules. This work marks a critical step toward realizing WGM laser probes (particles) for molecular sensing.

Herein, we will discuss a few possible directions for this work. First, the innovation of this work can be widely applied to different target molecules and assays, such as proteins, DNA, ELISA, and small molecules. The wavelengths of the donor and acceptor molecules can be customized to best suit the target of interest. Secondly, the concept of laser-sensing probe has great potential for intracellular or extracellular detection. However, the current size is still too large for regular cell function, thus it is necessary to scale down the probe to ~1 μm so that it will not cause unwanted effects within the cellular structures. Possible solution to this is to increase the refractive index of the laser probe. Hence the ability to achieve tiny lasing probes with specific sensing functions can be envisioned for diagnosis and cellular monitoring. Thirdly, we envision that our work will significantly contribute to fundamental biological or chemical research, particularly that related to conformational change and polarization studies of molecules. Additionally, other features of laser-based detection (e.g., high sensitivity, multiplex ability, and a high signal-to-noise ratio) can also be incorporated into the proposed system and analyzed.

4. Experimental Methods and Materials

Materials and chemicals

The dyes we used in this paper were purhchased from Sigma Aldrich and Tokyo Chemical Industry; they are as follows: Coumarin 6 (C6 M_w, 350.43 g/mol) (Sigma-Aldrich #442631), Nile Red (NR M_w,

318.37 g/mol) (Sigma-Aldrich #72485), Rhodamine B (RhB M_w, 479.07 g/mol) (Tokyo Chemical Industry #A5102), Rhodamine 6G (Sigma-Aldrich #83697), Sulforhodamine 101 acid chloride (TR M_w, 625.15 g/mol) (Sigma-Aldrich #S3388), Rhodamine B isothiocyanate (RhBITC M_w, 536.08 g/mol) (Sigma-Aldrich #283924) and R-Phycoerythrin (RPE M_w, 240 kD) (Sigma-Aldrich #52412). (3-aminopropyl) triethoxysilane (APTES) (Tokyo Chemical Industry #A0439) as silane coupling agent (M_w, 221.37 g/mol). 4-Cyano-4'-pentylbiphenyl purchased from Tokyo Chemical Industry (#C1550) as nematic liquid crystal (5CB), sodium dodecyl sulfate (SDS M_w, 288.38 g/mol) (Sigma-Aldrich #L3771) as surfactant. N-Hydroxysuccinimide (NHS M_w, 115.09 g/mol) (Sigma-Aldrich #130672) and N-(3-Dimethylaminopropyl)-N-ethylcarbodiimide hydrochloride (EDC M_w, 191.70 g/mol) (Sigma-Aldrich #03450) were purchased from Sigma Aldrich. For the LC microdroplet surface modified, we used the Poly(4-styrenesulfonic acid) solution (PSS M_w, 75000 g/mol) which was purchased from Sigma Aldrich (#561223).

Liquid crystal microdroplets preparation

To perpare the dye doped Liquid crystal (LC), 3.5 mg (10 µmol) of Coumarin 6 or 3.18 mg (10 µmol) NR was added to 500 µL of 5CB LC and then mixed on the vortex for 10 minutes. Final dye concentration in the LC is 20 mM. For perparing the LC microdroplets aqueous solution, 28.8 mg (0.1 mol) of SDS was added to 50 mL of PBS solution. The mixture was stirred magnetically for about 20 minutes at 1000 rpm to obtain a homogeneous SDS/PBS solution. To perpare the LC microdroplet emulsion, 10 µL of dye doped LC was added to 1 mL homogeneous SDS/PBS solution. The resulting

mixture was mixed on the vertex for 1 minute to produce a LC microdroplet emulsion. For the laser experiment, we choosed the LC microdroplets with diameter at 26 ± 1 μm.

Mounting microdroplets onto glass slides

For the glass slides, we first cleaned the glass slides using acetone before applying 2% v/v APTES/acetone for a period of 3 min. Then, we washed the slides with ethanol two times and washed them with water. Next, we dried the slides at 25°C for 12 h[35]. To obtain the solution, we added 30 mg (260 μmol) of NHS and 30 mg (156 μmol) of EDC into 5 mL of PBS solution and put glass slides into solution; we then added the solution to a petri dish and placed the glass slides into the solution. To immobilize the LC microdroplets on APTES modified slide cover glasses, the carboxylic groups of LC microdroplets were activated by adding LC microdroplet emulsion into petri dish which contained NHS and EDC dissolved PBS solution. Finally, the petri dishes were stored at room temperature for 12 hours.

Preparation of PSS-modified LC microdroplets and dye-coating LC microdroplets

First, 5CB microdroplets (10 μL) were prepared in the 1 mL SDS/PBS solution and subjected to sonication for 5 min. Second, solution replaced by 9 wt% Poly(4-styrenesulfonic acid) (PSS) solution following centrifugation at 5000 rpm for 4 min. Here PSS was used to fix the droplets due to negatively charged property. Then, we incubated the product at room temperature for 30 min. Following incubation, the LC microdroplets were washed by adding PBS solution and performing

centrifugation. Regarding the dye-coating process, 1 mL of RhB/PBS solution with a 50 μM concentration was added to LC microdroplets before it was subjected to slowly mixing for a period of 1 h. Finally, the microdroplets were washed with PBS solution three times to remove the unbound dye in the surrounding medium[36]. As a result, only those dye molecules that are coated on the microdroplet surface and form a monolayer of dye molecules.

Optical setup

An inverted microscopic system (Nikon Ti2) with 20X 0.4 NA objective was used to pump the liquid crystal microdroplets and collect light. Optical pumping was achieved by a pulsed ns-laser (EKSPLA PS8001DR) integrated with an optical parametric oscillator with (repitition rate: 50 Hz; pulse duration: 5 ns). According to respective absorption wavelength of fluorophores, the pump laser was tuned to 450 nm for C6 or 532 nm for NR. The beam diameter at the objective focal plane was approximately 16 μm. The collected light was transmitted to a charge-coupled device camera or an imaging spectrometer (Andor Kymera 328i and Newton 970 EMCCD). For measurements of fluorescence image, an integrated LED was used as the excitation source and imaged by color CCD (Basler acA1600-20uc) mounted on the inverted microscope.

Supporting Information

Supporting Information is available from the Wiley Online Library.

Acknowledgments

The authors would like to thank Professor Yu-Chieh Cheng at the National Taipei University of Science and Technology for instruction on liquid crystal laser fabrication. We would like to thank the lab support from Centre of Bio-Devices and Signal Analysis and Internal Grant NAP SUG - M4082308.040 from NTU.

Disclosures

The authors declare no conflicts of interest.

Received: ((will be filled in by the editorial staff))
Revised: ((will be filled in by the editorial staff))
Published online: ((will be filled in by the editorial staff))

References

1. Y. C. Chen, X. Fan, *Adv. Opt. Mater.* **2019,** *7* (11), 1900377.
2. X. Fan, S. H. Yun, *Nat. Methods* **2014,** *11*, 141-147.
3. V. D. Ta, S. Caixeiro, F. M. Fernandes, R. Sapienza, *Adv. Opt. Mater.* **2017,** *5* (8), 1601022.
4. A. Fernandez-Bravo, K. Yao, E. S. Barnard, N. J. Borys, E. S. Levy, B. Tian, C. A. Tajon, L. Moretti, M. V. Altoe, S. Aloni, K. Beketayev, F. Scotognella, E. Cohen. E. M. Chan, P. J. Schuck, *Nat. Nanotech.* **2018**, *13* (7), 572.
5. X. Li, Y. Qin, X. Tan, Y. C. Chen, Q. Chen, W. H. Weng, X. Wang, X. Fan, *ACS Photon.* **2019,** *6* (2), 531-537.
6. M. Humar, M. C. Gather, S. H. Yun, *Opt. Express* **2015,** *23*, 27865-27879.
7. C. P. Dietrich, A. Steude, L. Tropf, M. Schubert, N. M. Kronenberg, K. Ostermann, S. Höfling, M. C. Gather, *Sci. Adv.* **2016,** *2* (8), e1600666.
8. Y. C. Chen, X. Tan, Q. Sun, Q. Chen, W. Wang, X. Fan, *Nat. Biomed. Eng.* **2017,** *1* (9), 724-735.

9. T. Baba, *MRS Commun.* **2015,** *5* (4), 555-564.

10. Q. Chen, M. Ritt, S. Sivaramakrishnan, Y. Sun, X. Fan, *Lab Chip* **2014,** *14*, 4590-4595.

11. Y. C. Chen, Q. Chen, X. Fan, *Lab Chip* **2016,** *16* (12), 2228-2235.

12. Y. C. Chen, Q. Chen, X. Fan, *Optica* **2016,** *3* (8), 809-815.

13. N. Martino, S. J. J. Kwok, A. C. Liapis, S. Forward, H. Jang, H.-M. Kim, S. J. Wu, J. Wu, P. H. Dannenberg, S.-J. Jang, Y. H. Lee, S. H. Yun, *Nat. Photon.* **2019,** *(13)*, 720–727.

14. A. H. Fikouras, M. Schubert, M. Karl, J. D. Kumar, S. J. Powis, A. di Falco, M. C. Gather, *Nature Commun.* **2018,** *9* (1), 4817.

15. M.Humar, S. H. Yun, *Nat. Photon.* **2015,** *9* (9), 572-576.

16. Z. Lv, Z. Man, Z. Xu, C. Feng, Y. Yang, Q. Liao, X. Wang, L. Zheng, H. Fu, *ACS Appl. Mater. Interfaces* **2018,** *10* (39), 32981-32987.

17. G. Pirnat, M. Humar, I. Muševič, *Optics Exp.* **2018,** *26* (18), 22615-22625.

18. M. Humar, *Liquid Crystals* **2016,** *43* (13-15), 1937-1950.

19. M. Humar, A. Dobravec, X. Zhao, S. H. Yun, *Optica* **2017,** *4* (9), 1080-1085.

20. Z. Gao, W. Zhang, Y. Yan, J. Yi, H. Dong, K. Wang, J. Yao, Y. S. Zhao, *ACS Nano* **2018,** *12* (6), 5734–5740.

21. X. Wu, Q. Chen, P. Xu, Y. C. Chen, B. Wu, R. M. Coleman, L. Tong, X. Fan, *Nanoscale* **2018,** *10* (20), 9729-9735.

22. M. Schubert, A. Steude, P. Liehm, N. M. Kronenberg, M. Karl, E. C. Campbell, S. J. Powis, M. C. Gather, *Nano Lett.* **2015,** *15*, 5647-5652.

23. H.-J. Moon, G.-W. Park, S.-B. Lee, K. An, J.-H. Lee, *Appl. Phys. Lett.* **2004,** *84* (22), 4547-4549.

24. K. An, H.-J. Moon, *J. Phys. Soc. Jpn.* **2003,** *72* (4), 773-776.

25. Y.-S. Choi, H.-J. Moon, S. W. Kim, K. An, *J. Korean Phys. Soc.* **2001,** *39* (5), 928-931.

26. M. R. Foreman, J. D. Swaim, F. Vollmer, *Adv. Opt. Photon.* **2015,** *7*, 168-240.

27. F. Vollmer, S. Arnold, D. Keng, *Proc. Natl. Sci. Acad. USA* **2008,** *105*, 20701-20704.

28. M. D. Baaske, F. Vollmer, *Nat. Photonics* **2016,** *10* (11), 733.

29. Y. C. Chen, Q. Chen, X. Wu, X. Tan, J. Wang, X. Fan, *Lab Chip* **2018,** *18* (7), 1057-1065.

30. K. Wang, Z. Gao, W. Zhang, Y. Yan, H. Song, X. Lin, Z. Zhou, H. Meng, A. Xia, J. Yao, Y. S. Zhao, *Sci. Adv.* **2019,** *5* (6), eaaw2953.

31. K. Trofymchuk, A. Reisch, P. Didier, F. Fras, P. Gilliot, Y. Mely, A. S. Klymchenko, *Nat. Photonics* **2017,** *11* (10), 657.

32. N. Melnychuk, A. S. Klymchenko, *J. Am. Chem. Soc.* **2018,** *140* (34), 10856-10865.

33. A. Pieper, M. Hohgardt, M. Willich, D. A. Gacek, N. Hafi, D. Pfennig, A. Albrecht, P. J.Walla, *Nat. Commun.* **2018,** *9* (1), 666.

34. M. Aas, Q. Chen, A. Jonáš, A. Kiraz, X. Fan, *IEEE J. Sel. Top. Quantum Electron.* **2016,** *22* (4), 1-15.

35. Y. Huan, S. J. Park, K. C. Gupta, S.-Y. Park, I.-K. Kang, *RSC Adv.* **2017,** *7* (60), 37675-37688.

36. I. Verma, S. Sidiq, S. K. Pal, *ACS Omega* **2017,** *2* (11), 7936-7945.

37. S. Yang, Y. Wang, H. Sun, *Adv. Opt. Mater.* **2015,** *3* (9), 1136-1162.

38. J. R. Lakowicz, Springer Science & Business Media: 2013.

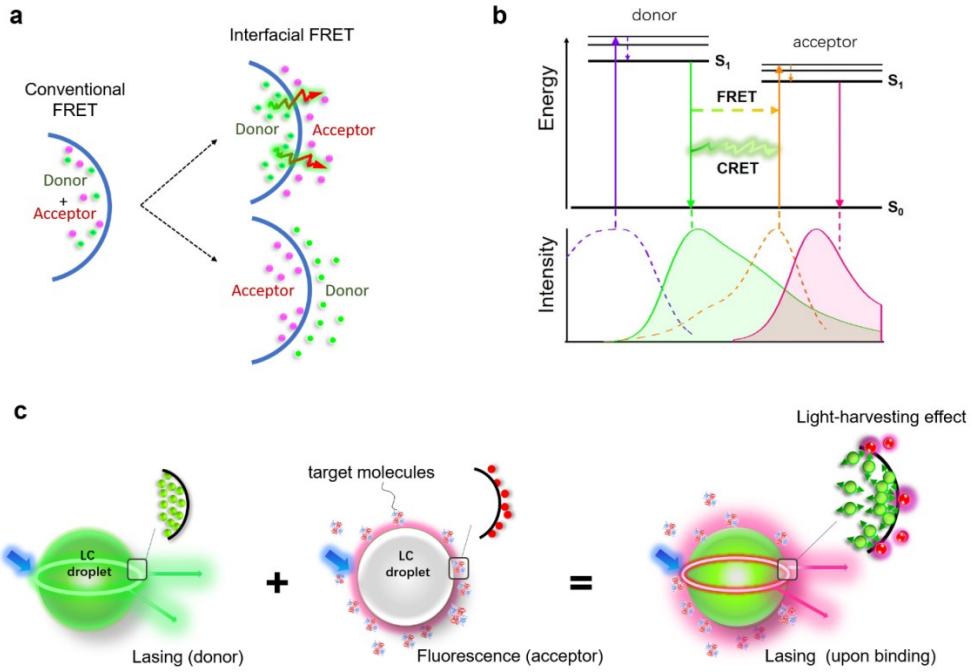

Figure 1. (a) Comparison of conventional FRET and interfacial FRET. The blue curve represents the cross-section of droplet interface. Configuration 1 (i.e., top-right configuration): donor and acceptor molecules within and outside of a liquid crystal WGM cavity, respectively. Configuration 2 (i.e., bottom-right configuration): donor and acceptor molecules outside and inside of a liquid crystal WGM cavity, respectively. **(b)** Diagram showing the transfer of energy from the donor molecule to the acceptor molecule; non-radiative FRET (dashed line) and strong radiative CRET (solid line) both contributes to laser emission. **(c)** Schematic diagram illustrating interfacial FRET laser function; highly concentrated donor molecules act as light-harvesting antenna to excite a low concentration of acceptor molecules. The green particles represent donor molecules doped in liquid crystal (LC) droplet, where Coumarin 6 was used in this work. The red particles represent target molecules (acceptor molecules with fluorescence emission) at the microdroplet surface or interface. Acceptor molecules used in this work includes Rhodamine B, Rhodamine 6G, Texas Red, Rhodamine B isothiocyanate, and R-phycoerythrin.

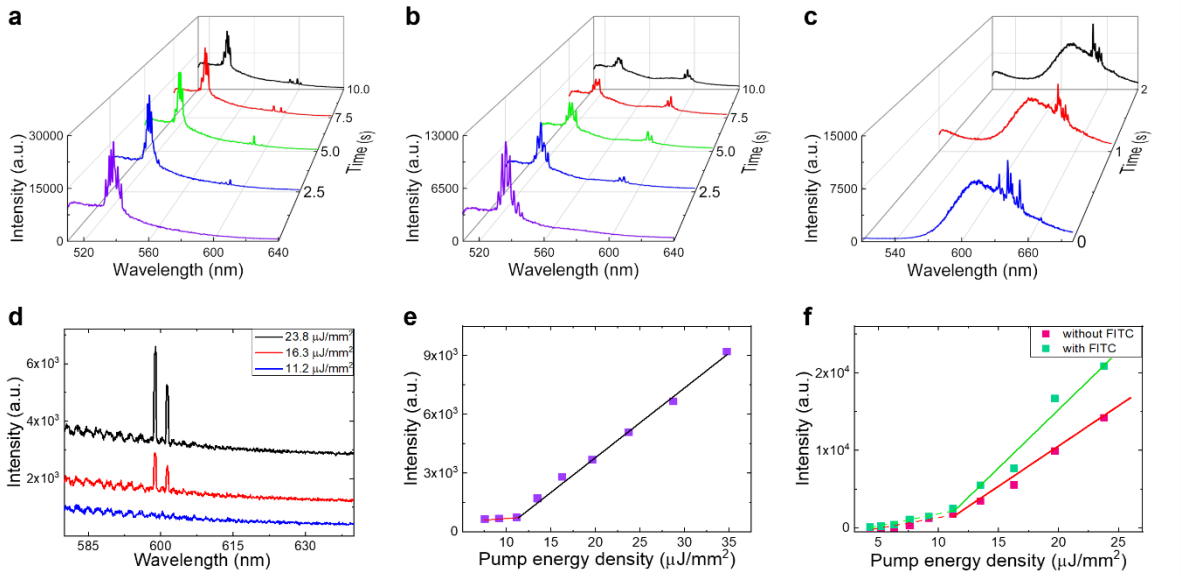

Figure 2. (**a–b**) Configuration 1: Dynamic lasing spectra of a fixed Coumarin 6 (C6, donor) microdroplet that were obtained after (**a**) 0.1-mM or (**b**) 0.5-mM Rhodamine B (RhB, acceptor) solution was added under the condition of the same pump energy. Each color represents a different time at which the lasing spectra was measured (excitation wavelength: 450 nm). (**c**) Configuration 2: Dynamic lasing spectra of a fixed Nile Red (NR, acceptor) microdroplet after adding 0.5-mM Fluorescein isothiocyanat (FITC, donor) solution under the condition of the same pump energy (excitation wavelength: 475 nm); each color represents a different time at which the lasing spectra was measured (unit: s). (**d**) Lasing spectra of the 0.1-mM RhB encompassing the C6 microdroplet, with relatively low pump energy densities; the curves have been vertically shifted for clarity. (**e**) Spectrally integrated RhB laser output as a function of the pump energy density extracted from the spectra shown in (**d**), where the wavelength range is 595–605 nm, and the solid line denotes a linear fit; the lasing threshold is approximately 12 μJ/mm^2. (**f**) Spectrally integrated NR laser output as a function of pump energy density (640–660 nm). Red line: NR microdroplet results for a 475-nm pump; green line: 475-nm pump results for an NR microdroplet with 0.5-mM FITC solution. The solid lines show linear fits; the lasing threshold is approximately 11.5 μJ/mm^2. Diameter of droplet= 26 μm. Donor concentration of microdroplet= 20 mM.

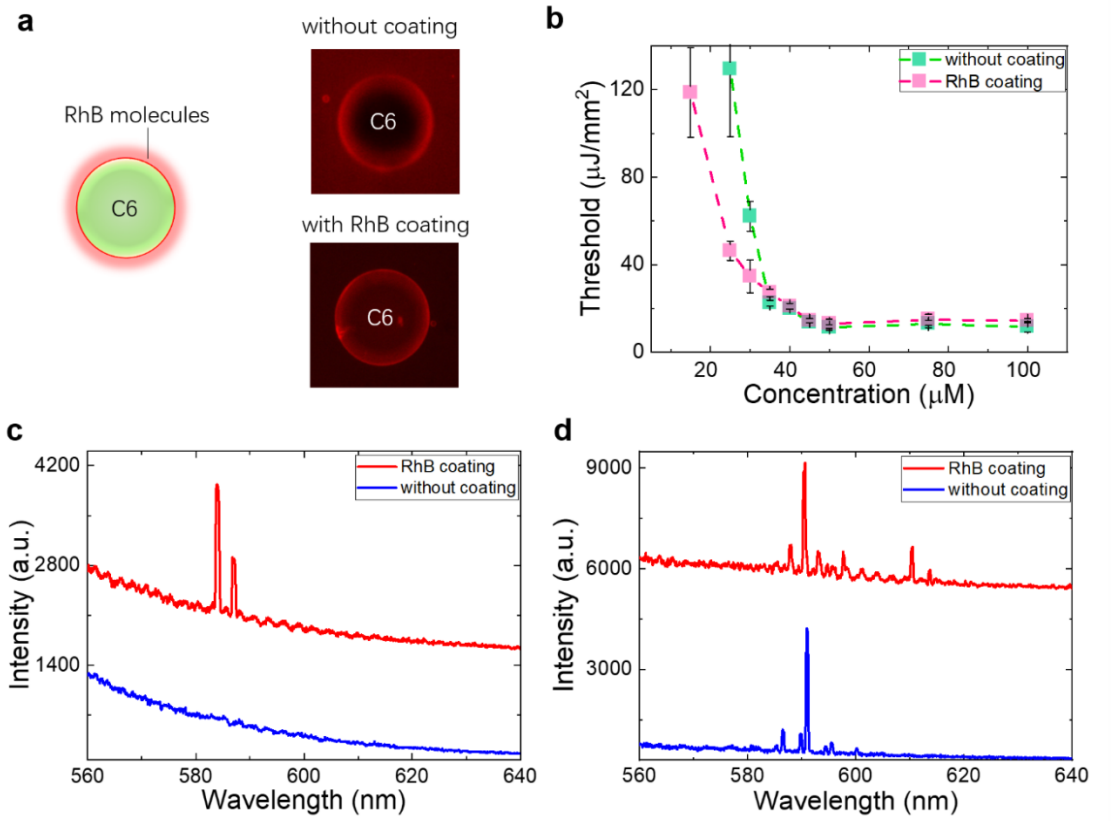

Figure 3. (a) Fluorescence image and schematic diagram of Rhodamine B (RhB)-coated liquid crystal microdroplet. The upper image shows a Coumarin 6 (C6) droplet that has been directly immersed in RhB solution (i.e., no coating process); the lower image shows a C6 droplet with a monolayer of RhB-coated molecules, as obtained after washing excessive dyes. (**b**) Interfacial FRET lasing threshold values as a function of concentration of the RhB solution surrounding the C6 microdroplet. Green boxes: microdroplet without RhB coating; pink boxes: RhB-coated microdroplet. The coated microdroplet was able to achieve lasing at a lower RhB concentration than the microdroplet without a coating. (**c**–**d**) Comparisons of FRET lasing peaks achieved by using the microdroplet with (red) and without (blue) coated RhB molecules (note that the pump energy was the same). The significance of the concentration of the RhB solution was investigated by using (**c**) 15 μM RhB and (**d**) 100 μM RhB; the curves have been vertically shifted for clarity. Diameter of droplet= 26 μm. Donor concentration of microdroplet= 20 mM.

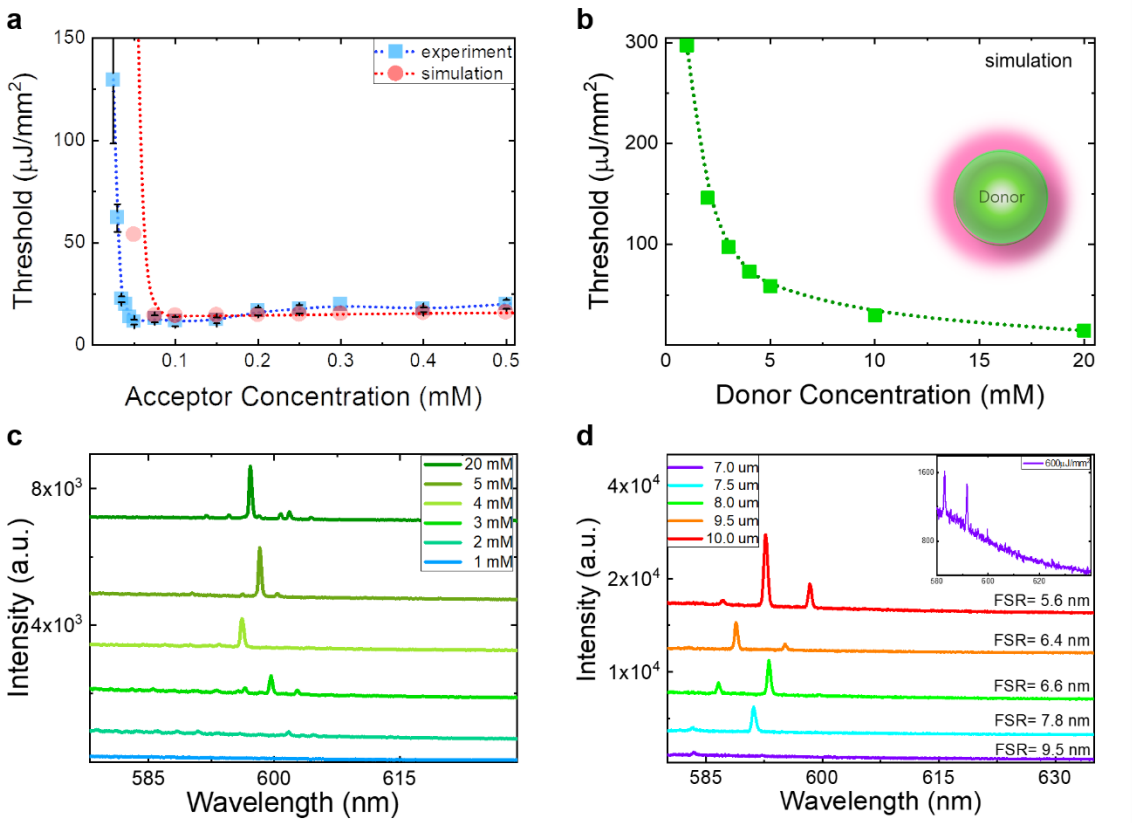

Figure 4. (a) Simulated and experimental interfacial FRET lasing threshold results for different Rhodamine B (RhB, acceptor) concentrations applied to a Coumarin 6 (C6, donor) microdroplet. Blue: experimental data; red: simulated data. **(b)** Simulated and experimental FRET lasing threshold results as a function of donor concentration (0.25-mM RhB concentration). For the simulated curve given in **(b)**, the threshold for 2 mM is 146.4 μJ/mm^2. **(c)** The experimental FRET lasing threshold results, as obtained under the condition of a fixed pump energy of approximately 150 μJ/mm^2 (experiment), for different C6 concentrations. **(d)** Lasing spectra of microdroplets of different sizes, the corresponding FSRs were calculated as labeled. The inset shows a zoomed-in view of the peak of the 7 μm diameter LC droplet at a higher pump energy. All curves have been vertically shifted for clarity.

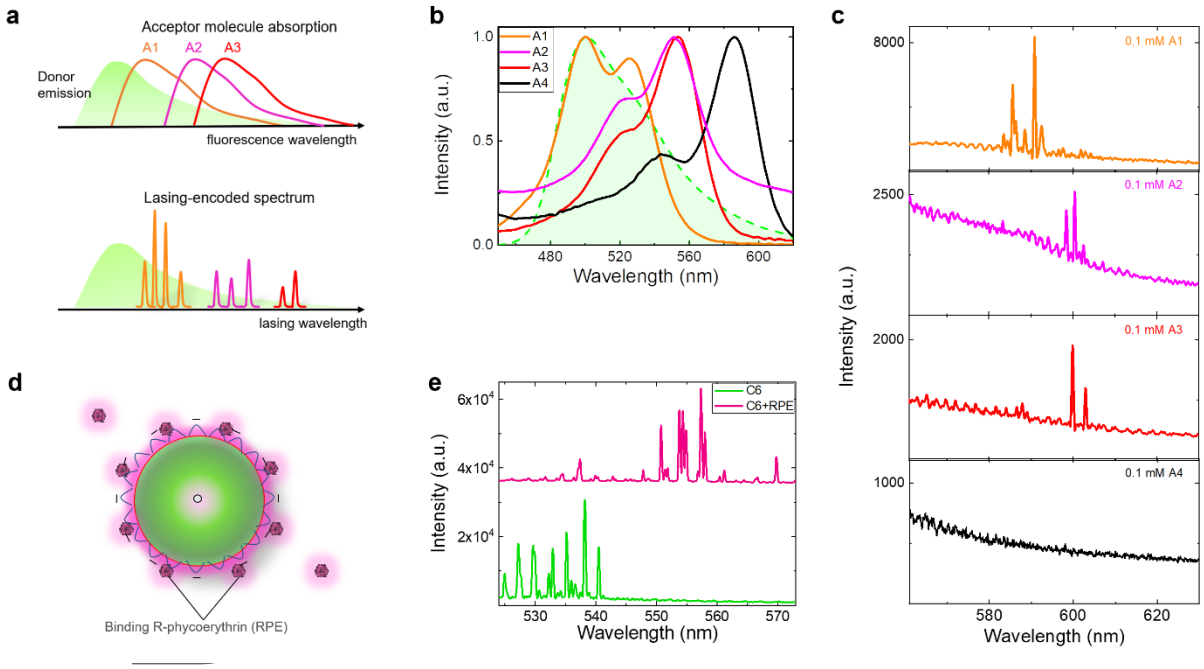

Figure 5. (a) Principle of lasing-encoded sensor based on different molecule absorption (A1, A2, A3 represents the absorption spectrum for different fluorescent molecules). The bottom panel shows the resultant lasing-based detection of respective molecules. **(b)** Normalized emission spectra of donor Coumarin 6 (green), applied with different acceptor molecules: Rhodamine 6G (orange, A1), Rhodamine B isothiocyanate (pink, A2), Rhodamine B (red, A3), and Texas Red (black, A4). **(c)** Interfacial lasing spectra of the four individual acceptor molecules corresponding to (b), as obtained under the condition of the pump energy density of 20 μJ/mm^2. The concentrations for all acceptor molecules was fixed at 0.1 mM. **(d)** Schematic diagram of R-phycoerythrin (RPE) molecules binding to a lasing microdroplet surface. **(e)** Magenta curve: lasing spectra for the RPE protein-based interfacial FRET laser; green curve: lasing spectra of the C6 microdroplet alone. The curves have been vertically shifted for clarity. Diameter of droplet= 26 μm. Donor concentration of C6 microdroplet= 20 mM.

We have proposed a novel concept to achieve active lasing-encoded biosensors by taking advantage of light-harvesting effect at the cavity interface, where interfacial molecular lasers based on cavity resonant energy transfer was demonstrated. This work marks a critical step of realizing WGM laser probes for biosensing, opening a new avenue in laser-based molecular sensing.